A fully Eulerian multiphase model of windblown sand coupled with morphodynamic evolution: Erosion, transport, deposition, and avalanching

Applied Mathematical Modelling 79 (2020) 68–84

Contents lists available at ScienceDirect

Applied Mathematical Modelling

journal homepage: www.elsevier.com/locate/apm

# A fully Eulerian multiphase model of windblown sand coupled with morphodynamic evolution: Erosion, transport, deposition, and avalanching

A. Lo Giudice [a,b,c,*], L. Preziosi [a,c]

[a] Department of Mathematical Sciences, Dipartimento di Eccellenza 2018-2022, Politecnico di Torino, Corso Duca degli Abruzzi 24, Turin 10129, Italy
[b] Optiflow, 160 Chemin de la Madrague-Ville, Marseille 13015, France
[c] Windblown Sand Modeling and Mitigation Joint Research, Development and Consulting Group, Italy

ARTICLE INFO

*Article history:*
Received 21 December 2018
Revised 10 May 2019
Accepted 25 July 2019
Available online 21 August 2019

*Keywords:*
Windblown sand
Multiphase flow
Morphodynamics
Transport phenomena

ABSTRACT

Modeling unsteady windblown sand dynamics requires not only treatment of the sand present in the air as a suspended constituent of a mixture but also consideration of erosion and sedimentation phenomena and consequently of the morphodynamic evolution of the sand-bed surface, including avalanching, especially in the presence of natural or human-built obstacles, artifacts, and infrastructures. With this aim in mind, we present a comprehensive multiphase model capable of accurately simulating all the physical phenomena mentioned above, producing satisfactory results, with reasonable computational effort. As test cases, two- and three-dimensional simulations of dune evolution are reported, as is windblown sand transport over a straight vertical wall. Examples of sand transport around other obstacles are given to show the flexibility of the model and its usefulness for such engineering applications.



## 1. Introduction

When wind blowing on a sandy surface, such as a beach or a dune in the desert, is sufficiently strong, sand particles are set in motion from the sand bed and are entrained in the air flow. Depending on their diameter, sand grains are then transported by different physical mechanisms: big grains start to roll (creep), medium-sized grains describe ballistic-like trajectories and impact again on the sand surface, triggering a chain reaction by colliding with other particles, a phenomenon known as saltation, while small grains are entrained by the wind, forming a very thin suspension that can transport sand dusts over large distances (see Fig. 1).

Among the transport mechanisms mentioned, saltation involves almost 80% of the total moving mass [1]. By sedimentation, sand grains accumulate in new downwind regions and pile up until the sand-bed surface reaches a slope that exceeds a critical repose angle. Above this angle avalanching occurs, redistributing the sedimented mass so that a new stable configuration is established. To model this quite complex physical phenomenon, it is crucial to consider all the aspects mentioned

* Corresponding author at: Optiflow, 160 Chemin de la Madrague-Ville, 13015 Marseille, France.
*E-mail addresses:* logiudice@optiflow.fr, andrea.logiudice@polito.it (A. Lo Giudice).

https://doi.org/10.1016/j.apm.2019.07.060

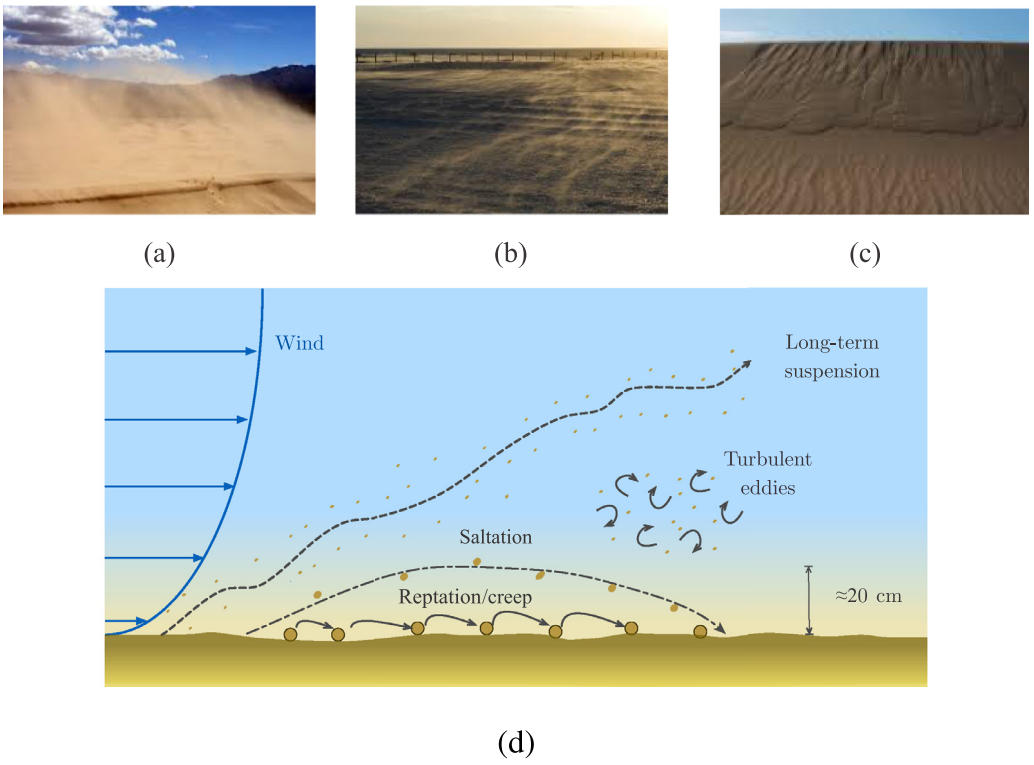


**Fig. 1.** Sand transport and morphodynamic evolution: (a) erosion and suspension, (b) saltation, (c) avalanching, and (d) transport mechanisms.

above. The aim of this work is to present a comprehensive mathematical and computational model capable of accurately simulating windblown sand transport, taking into account sand erosion, grain entrainment in the wind flow, deposition, and avalanches determining the morphodynamic evolution of the sand bed.

Historically, Bagnold [2] paved the way for the scientific investigation of windblown sand. However, only recently have computational approaches taken hold, although there were some early attempts in the 1980s (see, e.g., [3]). With the aim of modeling the motion of dunes, several authors (see, e.g., [4–9]) have proposed models for sand transport, most of them using perturbation theories and linearizations to evaluate wall shear stress, but without using multiphase coupling.

With respect to the existing literature, this article focuses on the complex multiphase fluid dynamics of the sand-air flow, in particular in the presence of natural (e.g., dunes) or human-built (e.g., barriers) artifacts, and on deducing a model that includes the mutual interaction of sand, air, and obstacles. Sand concentration in the air and the velocity of particles are the model's outcomes. This allows us to evaluate the transport of sand even when the suspension mode is crucial; for instance, in the presence of a barrier. In these situations the currently available models cannot be used because they solve transport of sand at ground level or inside a thin layer close to the ground, and therefore they cannot evaluate how much sand is entrained in the air and how much of this sand, carried by the wind, overcomes the obstacle.

Referring to Lo Giudice et al. [10] for a deeper review of the literature focusing mainly on fluid-dynamic aspects of windblown particulate transport, a first division of the mathematical models for windblown sand can be done by distinguishing between Eulerian–Lagrangian and fully Eulerian models. In both approaches air flow is treated using a continuum model, followed by working in an Eulerian framework, even though different models have been proposed; for example, Reynolds-averaged Navier–Stokes with one-equation turbulence closure [11] and two-equation [12–14] models, large eddy simulation [15–17], and a lattice Boltzmann approach [18].

On the other hand, regarding the solid phase, the former approach treats each sand particle as a discrete element, following it during its trajectories. A different coupling degree can be achieved by including different levels of interaction between particles and air, which can also include how the flow is affected by the presence of sand, and how the particles interact among themselves through interparticle collisions. The Lagrangian models also differ in the particle collision model, in the treatment of the particle-bed interaction, and in the level of coupling. For instance, Li et al. [16] modeled all the possible interactions using a four-way coupling discrete element method, while Xiao et al. [19] considered two particle size distributions (Gaussian and uniform). Unfortunately, Eulerian–Lagrangian models become computationally unfeasible or at least extremely costly for real environmental applications. They would require an enormous number of ordinary differential equations to be solved to compute all sand grain trajectories, jointly with the fluid dynamics for the air phase.

A different approach consists in working in the spirit of mixture theory and multiphase flows considering sand as a solid immiscible constituent dispersed in the air and described by mass and momentum balance equations. In this way, the

structure of the model is fully Eulerian. The first studies that tried to explore this modeling approach were those of Alhajraf [20] and Ji et al. [21]. In particular, Alhajraf [20] used both an Eulerian–Lagrangian approach and a fully Eulerian approach, and concluded that the latter is a good compromise between accuracy and computational time.

The present work extends the model presented in [22], with the aim of taking into account the main phenomena necessary to describe windblown sand (erosion, transport, deposition), coupling them with a morphodynamic evolution model of the sand surface, including the avalanche model presented in [23]. A crucial role is played by the erosion condition triggering the entire phenomenon (the interested reader is referred to Raffaele et al. [24] for a critical comparison of all the laws proposed in the literature done on a statistical basis).

In particular, special attention is given to the case of flows over inclined surfaces, characterizing not only dunes but also the interaction with other structures, generalizing the experimental relation proposed in [25] to the three-dimensional case. Finally, the comprehensive model is used to fully reproduce sand transport in desert areas in nonequilibrium conditions (i.e., when the sand-bed surface is constantly changing due to erosion and deposition). This is done both in natural conditions, such as in the presence of dunes, and in the presence of human-built obstacles.

Dune evolution can be considered as the reference test case of interest because it involves all the physical phenomena that contribute to sand transport together with the aerodynamics of a bluff body in the atmospheric boundary layer. For this reason it was selected here to show the capability of the model to resemble the morphology of a dune as the final result of the windblown transport process simulated.

As stated already, dune dynamics has already been studied by different authors, from both the pure aerodynamic point of view [26–31] and the morphodynamic point of view with different focuses: continuous models [5,9,32], barchans [33–35], parabolic and coastal dunes [36,37], martian dunes [38], linear dunes [39], instabilities [40], star dunes [41,42], and erosion [14,43].

On the basis of the work of Kroy et al. [5], Parteli et al. [44] proposed a three-dimensional model that is able to reproduce the shape evolution of different types of dunes. In these studies, the separation bubble generated by the dune is heuristically added in the lee, ignoring shear stress and sand fluxes in this region as a first approximation, making the model not directly applicable in different situations of interest; for instance, in the presence of obstacles [45–47]. Even in the case of a transverse dune, wind flow in the wake is highly nonlinear and has to be carefully solved (see [31], where the effects of boundary conditions on the shear stress patterns on the lee side of a transverse dune are analyzed). Moreover, sand transport and morphological evolution simulations in the presence of different sand mitigation measures (see [48] for an exhaustive list) would require at least a priori knowledge of the flow features, which will introduce a significant approximation on the primary cause of transport (i.e., the wind).

Differently, Zhou et al. [49] performed a three-dimensional numerical simulation of a downsized dune migration, based on wall shear stress calculations obtained from large eddy simulation. However, even though they computed erosion/deposition on the basis of wall shear stress, they did not explicitly solve suspension and saltation transport, and they focused only on the dune migration, solving an evolution equation of the ground terrain.

Dune migration was also simulated with use of *cellular automaton* algorithms with erosion, transport, and deposition phenomena treated using time-dependent stochastic interactions between cells of a lattice [50–53]. These models are useful to study long-term evolution of dune fields, but their aim is not to accurately compute local windblown sand transport, especially in the presence of obstacles. In the models mentioned above, the transport is solved at ground level (i.e., the sand flux is a quantity defined on the ground that accounts for all the mass transport above in the air).

This point is crucial when the wind profile and flow patterns induced by the presence of bluff bodies in the atmospheric boundary layer have to be accurately simulated, and when the assessment of sand particles entrained and transported in the air is the main purpose. For instance, this is the case of sandy wind around sand mitigation measures [45–48,54–57]. In particular, the flow patterns induced are able to entrain particles and to transport them with saltation and suspension modes. This work is intended to present a model capable of reproducing windblown transport also in such situations.

This article is organized as follows. In Section 2 the mathematical model for both phases is presented with particular attention to the derivation of the evolution equation for the bed level surface and its coupling with the avalanche model. Section 3 is devoted to simulations: First the model is tested with a two-dimensional case of a transverse dune and a three-dimensional simulation of evolution of a sand pile from an initial symmetric Gaussian to a barchan-like shape. After verification of the model behavior in these well-known configurations, a simulation of windblown sand around a vertical wall is reported, together with other examples of particle transport around different sand mitigation measures to show the area of applications of our study.

Attention is paid to the effects of the dependence of the law of erosion on the slope, to the description of the wind flow patterns around the artifacts, and to the mutual interaction wind-sand obstacles. The final section presents some conclusions and remarks.

## 2. Mathematical modeling

Sandy wind is modeled as a multiphase system constituted by the air (the carrying phase) and sand (the dispersed phase). Regarding the former, atmospheric boundary layer flows require the modeling of unsteady incompressible, turbulent flows. For the physical problem considered and the applications, we are interested in the long-term behavior of sand transport, which is mainly due to mean wind flux because sand mass transport occurs on a much longer timescale than the

characteristic timescales for turbulence. For this reason, we model the air phase using unsteady Reynolds-averaged Navier–Stokes equations coupled with the shear stress transport (SST) formulation of the $k-\omega$ turbulence model [58,59] to close the system of equations. With respect to $k-\epsilon$ models, $k-\omega$ SST performs better in the presence of flow separation and adverse pressure gradients [60].

The Reynolds-averaged approach with the selected turbulence model has already been used for dune aerodynamics analysis [29,31] and for bluff-body aerodynamics in deserts [47]. The complete set of equations reads

$$\begin{cases} \nabla\cdot\overline{\mathbf{u}}_f = 0, \\ \dfrac{\partial\overline{\mathbf{u}}_f}{\partial t} + \overline{\mathbf{u}}_f\cdot\nabla\overline{\mathbf{u}}_f = -\dfrac{1}{\hat{\rho}_f}\nabla\overline{p} + \nabla\cdot\left[(\nu_f+\nu_t)\nabla\overline{\mathbf{u}}_f\right], \\ \dfrac{\partial k}{\partial t} + \nabla\cdot(k\overline{\mathbf{u}}_f) = \nabla\cdot[(\sigma_k\nu_f+\nu)\nabla k] + \tilde{P}_k - \beta^* k\omega, \\ \dfrac{\partial\omega}{\partial t} + \nabla\cdot(\omega\overline{\mathbf{u}}_f) = \nabla\cdot[(\sigma_\omega\nu_f+\nu)\nabla\omega] + \alpha\dfrac{\omega}{k}P_k - \beta\omega^2 + (1-F_1)\dfrac{2\sigma_\omega}{\omega}\nabla k\cdot\nabla\omega, \end{cases} \tag{1}$$

where $\hat{\rho}_f$ is the air density, $\overline{\mathbf{u}}_f$ is the averaged fluid velocity, $\overline{p}$ is the averaged pressure, $k$ is the turbulent kinetic energy, $\omega$ is its specific dissipation rate, $\nu_f$ is the kinematic viscosity, and $\nu_t$ is the so-called turbulent kinematic viscosity. The kinetic energy production term $\tilde{P}_k$ is modeled by introducing a production threshold to prevent the buildup of turbulence in stagnation regions:

$$\tilde{P}_k = \min(P_k, 10\beta^* k\omega), \quad \text{where} \quad P_k \approx 2\nu_t\mathbf{D}\cdot\nabla\overline{\mathbf{u}}_f,$$

where $\mathbf{D} = \frac{1}{2}(\nabla\overline{\mathbf{u}}_f + \nabla\overline{\mathbf{u}}_f^{\mathrm{T}})$ is the strain rate tensor. For conciseness, the definition of the blending function $F_1$ and the values of the model constants are omitted herein but can be found in [59].

The dispersed phase is considered as a passive scalar modeled by the conservation equation for sand volume fraction $\phi_s$:

$$\frac{\partial\phi_s}{\partial t} + \nabla\cdot\mathbf{q} = 0, \tag{2}$$

where the flux $\mathbf{q}$ is the combination of advection by wind, sedimentation effects, and diffusive flux due to random collisions,

$$\mathbf{q} = \mathbf{u}_{tr}\phi_s + \mathbf{u}_{sed}\phi_s - \nu_{eff}\phi_s^{k-1}\nabla\phi_s, \tag{3}$$

with $k\geq 1$. $\mathbf{u}_{tr}$ is the transport velocity of the solid constituent induced by wind (the advection field), $\mathbf{u}_{sed}$ is the vertical component of velocity due to gravity, and $\nu_{eff}$ is an effective viscosity. The order of magnitude of the saltation layer on a flat plane is given by the ratio $\nu_{eff}/u_{sed}$.

As far as the effect of the wind is concerned, following the discussion in [22,61], $\mathbf{u}_{tr}$ is taken to be proportional to the wind velocity $\mathbf{u}_f$ according to experimental data.

As stated in [22], the settling velocity can be obtained by plotting the experimental relationship between the particle Reynolds number and drag given, for instance, in [62] in terms of a relationship between the grain size and the particle Reynolds number $Re_p = \frac{u_r d}{\nu_f}$, where $u_r$ is the particle sedimenting velocity and $d$ is the particle diameter (see also [63–65]).

Finally, through the effective viscosity $\nu_{eff}$ the last term takes into account the mixing-diffusive contribution due to the air viscosity $\nu_f$ to the turbulent viscosity $\nu_t$ and to the random collisional interactions $\nu_s$. Preziosi et al. [22] showed that $\nu_s = \nu_s(I\!I_{\mathbf{D}})$, where $I\!I_{\mathbf{D}}$ is the second invariant of the rate of strain tensor $\mathbf{D}$. In particular, we take $\nu_s = A(2\sqrt{I\!I_{\mathbf{D}}})^\beta$, where $A$ and $\beta$ are model parameters. This formulation implies that $\nu_s$ is an objective function (i.e., it does not depend on the reference frame).

### 2.1. Boundary conditions with slope effects

As already mentioned, one of the crucial mechanisms in sand transport, actually the triggering one, is erosion. It quantifies the amount of sand entrained by the wind. The phenomenon has been studied from the experimental point of view by several authors (see, e.g., [2,66]) and the difference between the proposed laws was studied in detail in [24]. From the mathematical point of view, this phenomenon enters the model as a boundary condition to be applied at the sand bed to solve the dispersed-phase equation.

As already mentioned, erosion occurs if the wall shear stress at the boundary is larger than a threshold value. Otherwise, the boundary condition is $\nabla\phi_s\cdot\mathbf{n} = 0$, which means that no diffusive flux is present and the total outgoing sand flux is the advective flux: $\phi_s(\mathbf{u}_s+\mathbf{u}_w)\cdot\mathbf{n}$.

Otherwise, one has an influx that depends on the difference between the shear stress and a threshold value. For instance, the vertical flux expression obtained by Ho et al. [67–69] by experiments on saltating grains is

$$-\nu_{eff}\phi_s^{k-1}\nabla\phi_s\cdot\mathbf{n} = A_H\hat{\rho}_f\sqrt{\frac{d}{g}}(u^{*^2} - u_t^{*^2})_+,$$

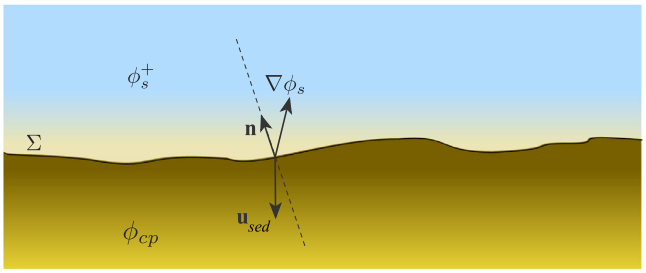


**Fig. 2.** Sand-bed interface scheme.

where $A_H$ depends on the physical properties of the sand and $(f)_+ := (f + |f|)/2$ stands for the positive part of $f$. In this expression the shear velocity $u^*$ is used instead of the wall shear stress $\boldsymbol{\tau}$. It is defined as $u^* = \sqrt{\frac{|\boldsymbol{\tau}|}{\rho_f}}$.

However, as reported in [70], the influence of the slopes on the friction velocity is not negligible. Gravity acts for or against erosion, according to the wind flow direction and the surface slope. To include such an effect, the following empirical modification was proposed in [25] for two-dimensional problems:

$$u_t^* = u_{t,0}^* \sqrt{\cos\vartheta + \frac{\sin\vartheta}{\tan\theta_{cr}}} = u_{t,0}^* \sqrt{\frac{\sin(\vartheta + \theta_{cr})}{\sin\theta_{cr}}}, \tag{4}$$

where $u_{t,0}^*$ is the friction velocity on a flat plane, $\vartheta$ is the local inclination of the surface, and $\theta_{cr}$ is the repose angle. With this modification, which holds for $\vartheta \in [-\theta_{cr}, \min\{\theta_{cr}, \pi - \theta_{cr}\}]$, the threshold velocity $u_t^*$ is amplified uphill, while it is reduced downhill, vanishing when the downhill angle is equal to $\theta_{cr}$ (i.e., $\vartheta = -\theta_{cr}$).

The relationship can be generalized to a three-dimensional problem by assuming that the lifting mechanism is affected by the dynamics in the vertical plane containing the local direction of the wall shear stress:

$$\boldsymbol{\tau} = 2\mu[\mathbf{D}\mathbf{n} - (\mathbf{n}\cdot\mathbf{D}\mathbf{n})\mathbf{n}] = \mu\frac{\partial \mathbf{u}_\parallel}{\partial \mathbf{n}} = \mu\mathbf{n}\cdot\nabla\mathbf{u}_\parallel,$$

where $\mathbf{u}_\parallel$ is the component of the velocity parallel to the sand bed. Hence, the effective impinging angle to be used in Eq. (4) is given by

$$\sin\vartheta = \hat{\boldsymbol{\tau}}\cdot\hat{\mathbf{k}}, \quad \hat{\boldsymbol{\tau}} = \frac{\boldsymbol{\tau}}{|\boldsymbol{\tau}|},$$

resulting in

$$u_t^*(x,t) = u_{t,0}^* \sqrt{\sqrt{1 - (\hat{\boldsymbol{\tau}}\cdot\hat{\mathbf{k}})^2} + \frac{\hat{\boldsymbol{\tau}}\cdot\hat{\mathbf{k}}}{\tan\theta_{cr}}}. \tag{5}$$

If $\boldsymbol{\tau}\cdot\hat{\mathbf{k}} = 0$ (e.g., if the wind flows along a transverse dune), then $\vartheta = 0$, so the threshold velocity is the same as for a flow over a flat plane. If, instead, for instance, the wind blows perpendicularly to the axis of a transverse dune, then $\boldsymbol{\tau}\cdot\hat{\mathbf{k}}$ is the sine of the slope of the transverse dune and Eq. (4) is recovered.

### *2.2. Evolution of the sand-bed surface: erosion, sedimentation, and avalanches*

Erosion and sedimentation phenomena continuously alter the shape of the sand-bed surface (Fig. 2). From the modeling point of view this means that the turbulence equations (1) and the equations for the solid phase (2) have to be integrated in a time-dependent domain and one needs to provide an evolution equation for the free boundary that will describe the morphological changes. From a computational point of view, the new ground configuration is also used to compute the ground displacement field to be applied by a front tracking approach and then mesh deformation.

To obtain an evolution equation for the sand-bed surface, it is sufficient to require continuity of sand flux across the nonmaterial interface $\Sigma$, which represents the ground level:

$$[\![(\mathbf{q} - \phi_s\mathbf{v}_\Sigma^{ED})\cdot\mathbf{n}]\!] = 0,$$

where $\mathbf{v}_\Sigma^{ED}$ is the descending or ascending velocity due to erosion or sedimentation.

Thus,

$$[\![(\mathbf{u}_{tr}\phi_s + \mathbf{u}_{sed}\phi_s - \nu_{eff}\phi_s^{k-1}\nabla\phi_s - \phi_s\mathbf{v}_\Sigma^{ED})\cdot\mathbf{n}]\!] = 0.$$

Bearing in mind that on the sand-bed side $\mathbf{u}_{tr}^- = \mathbf{u}_{sed}^- = 0$ and $\phi_s^- = \phi_{cp}$, the close-packing volume ratio, one has

$$(\mathbf{u}_{tr}\phi_s^+ + \mathbf{u}_{sed}\phi_s^+ - \nu_{eff}(\phi_s^+)^{k-1}\nabla\phi_s^+ - \phi_s^+\mathbf{v}_\Sigma^{ED})\cdot\mathbf{n} = (-\phi_{cp}\mathbf{v}_\Sigma^{ED})\cdot\mathbf{n}.$$

Reorganizing and dropping + indices finally gives

$$\mathbf{v}_{\Sigma}^{ED} \cdot \mathbf{n} = -\frac{1}{\phi_{cp} - \phi_s}(\phi_s \mathbf{u}_{tr} + \phi_s \mathbf{u}_{sed} - \nu_{eff}\phi_s^{k-1}\nabla\phi_s) \cdot \mathbf{n} = D + E, \tag{6}$$

where

$$D = -\frac{\phi_s(\mathbf{u}_{tr} + \mathbf{u}_{sed}) \cdot \mathbf{n}}{\phi_{cp} - \phi_s}$$

and

$$E = \frac{\nu_{eff}\phi_s^{k-1}\nabla\phi_s \cdot \mathbf{n}}{\phi_{cp} - \phi_s}$$

are the deposition and erosion velocity, respectively. Typically the former is positive and the latter is negative. If deposition prevails over erosion, then the bed-surface velocity is along the normal, which means that the ground level rises. In contrast, if erosion prevails, then the ground level lowers.

We recall that, in principle, sand grains can also move and roll along the sand-bed surface, contributing to the redistribution of mass and therefore to its evolution. This is due to creep, reptation, and avalanching. Creep and reptation contributions were included in other studies (e.g., [49], where reptation flux is proportional to saltation flux, while creep is function of the shear velocity $u^*$). However, for large amounts of mass transport, the contributions of these phenomena to morphological evolution of the ground surface are negligible compared with the contributions of saltation and avalanching, and for these reasons they are not considered here and in most of the literature.

Regarding avalanching, the sliding of sand grains is triggered when the slope of the accumulated (or eroded) sand exceeds a critical angle of repose $\theta_{cr}$, which in the case of dry sand is approximately 32°–34°. In light of the application of sand transport in the desert and in particular to dune dynamics, avalanching locally acts to modify slightly supercritical configurations formed by the transfer of sand eroded from upwind locations and deposited on the downwind side of the dune. Ignoring avalanching would then lead to unphysical configurations.

Lo Giudice et al. [23] derived a mechanical-based model called the *degenerate parabolic sliding model* for sand slides, and provided several numerical simulations with different boundary conditions as well as validation with experimental results from different authors. The evolution equation for the sand-bed surface height $h$ is

$$\frac{\partial h}{\partial t} = \nu_{av}\nabla \cdot \left[\frac{(|\nabla h| - \tan\theta_{cr})_+}{\sqrt{1 + |\nabla h|^2}}\frac{\nabla h}{|\nabla h|}\right], \tag{7}$$

where $\nu_{av}$ is related to the adhesivity properties of the particular granular material considered and determines the sliding time of the avalanches, once they are triggered. The square brackets contain the positive part of a function of the unknown that acts as a trigger of the avalanche flux and then for the evolution of the sand profile.

Including the erosion-deposition contribution $\mathbf{v}_{\Sigma}^{ED} \cdot \mathbf{n}$ in Eq. (7), one gets the complete evolution equation for $h$:

$$\frac{\partial h}{\partial t} = \nu_{av}\nabla \cdot \left[\frac{(|\nabla h| - \tan\theta_{cr})_+}{\sqrt{1 + |\nabla h|^2}}\frac{\nabla h}{|\nabla h|}\right] + D + E, \tag{8}$$

which is a modified Exner equation [71], a sediment mass balance equation developed for river morphology.

## 3. Numerical simulations

In this section we test the complete transport model in three different cases:

1. *The motion of a two-dimensional transverse dune.* This classical case was selected to verify if the model accurately reproduces the main transport processes that lead to the advancement of a transverse dune.
2. *Evolution of a sand pile into a barchan.* This configuration was selected to verify if the simulated transport process in a three-dimensional domain is able to lead to a coherent evolution of a pile into a barchan. In particular, in this case the generalized formula (5) for $u_t^*$ is used to take into account the effective angle between the wind and the local steepest slope direction.
3. *Windblown sand transport hindered by a vertical wall and interaction with other obstacles.* This last case was selected to show the applicability of the model in cases with nonstandard boundaries. In particular, these cases are significant because they show that the model is capable of dealing with situations of civil engineering interest in which suspension transport becomes crucial, and air-sand interaction is not straightforward and plays a central role in the sand transport mechanism, so it needs to be explicitly simulated.

The simulations were performed on a 10-processor cluster. Two-dimensional and three-dimensional dune simulations require 2 and 4 days, respectively. Specifically focusing on performance, Canuto and Lo Giudice [72] recently developed a scheme to accelerate considerably numerical simulations of this kind by adapting the discretization time according to the local features of the flow by means of an ad hoc domain decomposition method. The numerical scheme has been studied from the point of view of both accuracy and stability.

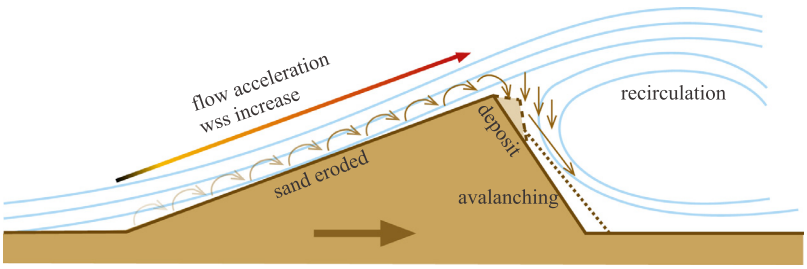


**Fig. 3.** Dune translation motion. Along the upwind face the wind accelerates. Hence, wall shear stress (wss) and therefore erosion increase. Sand deposits in the recirculation zone, also triggering avalanches. As a final result, the dune moves to the right.

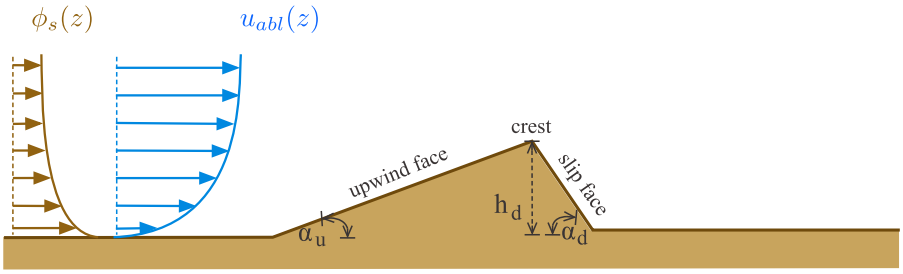


**Fig. 4.** Simulation setup. The wind blows from left to right. Inlet profiles for $\phi_s$ and $u_f$ are sketched in brown and blue, respectively. The dune reported represents the initial configuration: $h_d = 1$ m, $\alpha_u = 14°$, $\alpha_d = 30°$. (For interpretation of the references to color in this figure legend, the reader is referred to the web version of this article.)

### 3.1. Two-dimensional transverse dune

As a first case, we considered a classical setup to qualitatively test the complete erosion-transport-sedimentation-avalanching model with a well-known configuration already studied with dedicated models (e.g., [5,9]). We will focus on sand transport around a two-dimensional dune (representing a section of an eolian transverse dune) and its migration. As already stated, this is a reference test case of interest because it involves all the physical phenomena contributing to sand transport together with the aerodynamics of a bluff body in the atmospheric boundary layer. With respect to previous studies, we focus on fluid-dynamic behavior of the multiphase flow, and in particular on the coupling between air and sand transport, rather than on the long-term evolution of the dune.

In this setup the movement is the result of mass transfer from the soil to the air and then back to the soil. Dune translation is the final effect of the interaction of different phenomena, as schematized in Fig. 3. The incoming wind reaching the upwind face of the dune accelerates while approaching the crest. Consequently, it applies a growing shear stress on the sand surface, increasing the number of saltating particles and therefore erosion. Overcoming the crest, sand grains arrive in an air recirculation zone, in which the wind is much less energetic, and it does not exert a sufficiently strong shear stress to trigger erosion on the leeward side of the dune and to keep bigger grains entrained in the flow. Therefore, particles deposit starting from the region closer to the crest on the downwind side, which is also characterized by the presence of a stagnation point. Sand then progressively accumulates, and when the slope exceeds the critical repose angle, mass slides down, forming small avalanches that redistribute the mass in a subcritical manner. For this reason this side is also called the *slip face*. Looking at the global behavior, we see that the overall effect is that the dune moves downwind. We anticipate that the simulation is able to catch all the features just mentioned.

The simulation setup is sketched in Fig. 4. At the inlet we impose a logarithmic law for the mean wind speed profile,

$$\bar{u}_{f,x}(x_0, t) := u_{abl}(z) = U_{ref} \log\left(\frac{z + z_0}{z_0}\right),$$

and a decreasing exponential profile computed from a steady-state simulation for the sand volume ratio $\phi_s$. In addition, for the turbulence quantities $k$ and $\omega$ we prescribe a Richards–Norris profile [73]. At the outlet, zero-gradient boundary conditions are imposed for all the quantities, except for pressure, which is set to a reference value. At the ground, a no-slip condition is used for the velocity.

The aerodynamic roughness of the ground surface is taken into account by our using sand-grain roughness wall functions [74] at the ground surface. The equivalent sand-grain roughness height is expressed as $k_s = 9.793 z_{0g}/C_s$, where $C_s = 0.5$ is the roughness constant and $z_{0g}$ is the aerodynamic roughness of the ground surface. In [31] the fluid-dynamic model was validated against experimental results for analogous aerodynamic problems.

At each time step, after solving both phases, we update the domain to the new configuration obtained from Eq. (8).

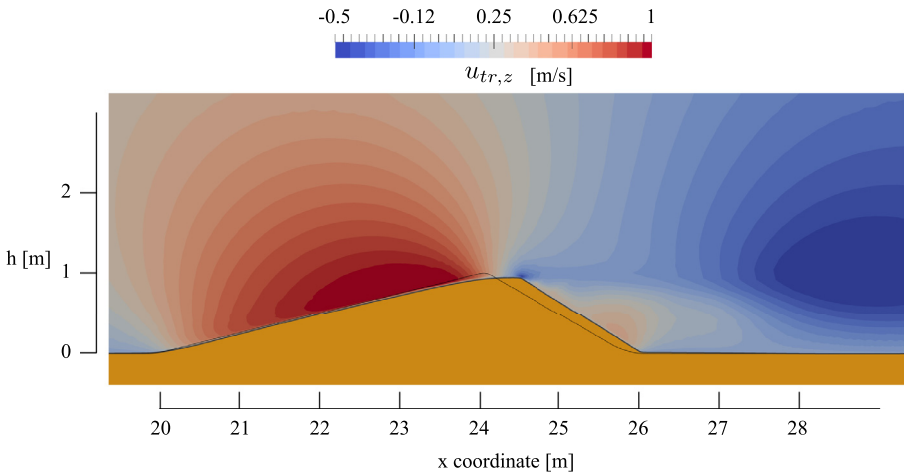


**Fig. 5.** Vertical sand speed contours $u_{s,z}$ at $t = 600$ s. The initial dune shape is shown in black.

**Table 1**
Saltation layer thickness at $t = 600$ s.

| Position | Saltation layer height (m) |
|---|---|
| Upwind flat zone (before reaching the dune) | 0.19 |
| After dune upwind toe | 0.24 |
| Middle dune upwind face | 0.26 |
| Close to the crest | 0.27 |

Numerical integration was performed with the finite volume open source code OpenFOAM®. In particular, in the following we accurately analyze the simulated results from both the aerodynamic point of view and the morphodynamic point of view.

In Fig. 5 the contour plots of the vertical velocity of sand are reported. Over the upwind face, the velocity points upward because of the ramp effect produced by the dune, which induces a positive vertical component. The same slightly happens close to the slip face because of the presence of a clockwise recirculation bubble.

Fig. 6 (a) shows the volume ratio $\phi_s$ close to the dune and the erosion-sedimentation balance $v_\Sigma^{ED}$ on the sand surface at $t = 600$ s. The black line in Figs. 5 and 6 represents the initial dune configuration. The saltation layer is clearly visible and its thickness, defined as the height $h_s$ such that

$$\int_0^{h_s} \phi_s(z)dz = 0.95 \int_0^{\infty} \phi_s(z)dz, \tag{9}$$

is quantitatively reported in Table 1 and increases along the dune upwind face.

It is worth pointing out that, differently from other models (see, e.g., [32]), the saltation layer height is not a model parameter but is a result of the balance between diffusion due to particle collision and the effect of gravity. The same consideration holds for the so-called *saturation length* studied in [22].

From a morphological point of view, in the upwind region erosion flux is bigger than sedimentation flux, and it has its maximum close to the dune crest (see the sand-air edge in Fig. 6(a)). It shows the same trend as the saltation layer thickness: the greater the erosion, the greater the amount of sand entrained by wind. Looking at the zoomed window on the crest, we can clearly see the wind smoothing effect: the initial spiky angle has been flattened because of the increased erosion flux. Moreover, it is interesting to note a thin layer of sand in the air after the slip face (highlighted in the zoomed zone at the bottom of Fig. 6(a)), inside the recirculation zone. This mass is ignored by models in which the recirculation bubble is heuristically placed behind the dune and in this zone a negligible shear stress at the ground is considered.

Looking at Fig. 6(a), we see that on the slip face $v_\Sigma^{ED}$ is positive, which means that sedimentation is occurring. Sand grains tends to fall and deposit immediately after the dune ridge. This is because this zone corresponds to the wind flow stagnation zone. Progressive accumulation of sand leads to a slope that exceeds the critical slope, and therefore avalanches can start to lower the slope angle to its repose value $\tilde{\theta}$. This is clearly visible in Fig. 6(b) from looking at the slope after the crest, which at $t = 600$ s has reached the critical angle of 32°.

After the slip face, there is a zone in which no saltation occurs. This is because there is a recirculation bubble with low wind velocity, visible in Fig. 6(b), which plots the horizontal component contour of the wind velocity.

To analyze the evolution in time, in Fig. 7 the dune profile (yellow), the local slope (blue line), and $v_\Sigma^{ED}$ (green line) are plotted at different time steps. After 100 s, the slope has reached the critical value just after the dune crest. This is because in this zone the sedimentation is maximum, as it is a preferential accumulation area where avalanches start forming, re-

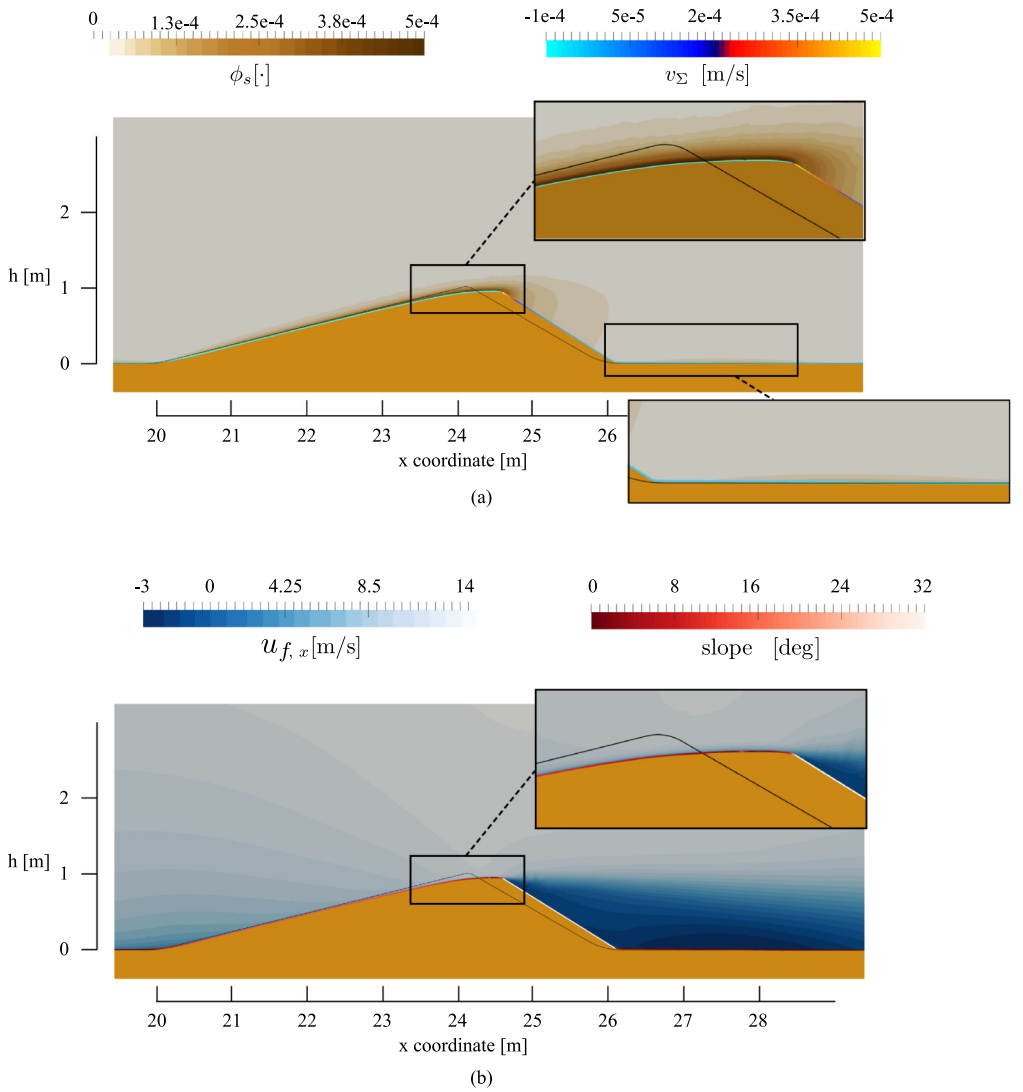


**Fig. 6.** Dune configuration at $t = 600$ s: (a) volume ratio $\phi_s$ contours (brown) and sand flux on the ground surface (colors); (b) $\bar{u}_{f,x}$ contour and slope of the ground surface. The initial dune shape is shown in black. (For interpretation of the references to color in this figure legend, the reader is referred to the web version of this article.)

distributing the mass downhill, eventually contributing to the advancement of the dune. After about $t = 250$ s the entire downwind slope has reached the threshold value and eventually moves as a traveling wave (see also Fig. 8). Looking at the last time step, we see a small accumulation zone is arising at the base of the slip face (it is also shown in Figs. 5 and 6).

Concerning the erosion-deposition phenomenon, it is worth stressing the following aspects:

- Far from the dune, both to the left and to the right, there is equilibrium between erosion and deposition, resulting in $v_\Sigma^{ED} \approx 0$.
- Approaching the dune, erosion starts to prevail quite fast and consequently $v_\Sigma^{ED} < 0$; at $t = 150$ s, $v_\Sigma^{ED}$ reaches its minimum just before the sand crest, while after an initial transient, it achieves an almost uniform value along the upwind face.
- Crossing the dune crest, there is a jump between erosion and deposition, as expected.

At the brink, the sand-bed velocity exhibits a peak: this is due to the presence of the sharp edge close to the crest, especially at the beginning of the simulation. The peak tends to lower after the initial transient, as the dune approaches a smoother configuration. However, in that zone, deposition is maximum because the shear stress goes to zero at the stagnation point.

From $x = 28$ m until $x = 29$ m is it possible to observe a mild erosion zone ($v_\Sigma^{ED}$ is negative). As already stated in the literature preceding this paper, the details of the phenomenon behind the dune are approximated by models that do not solve for the wind flow field.

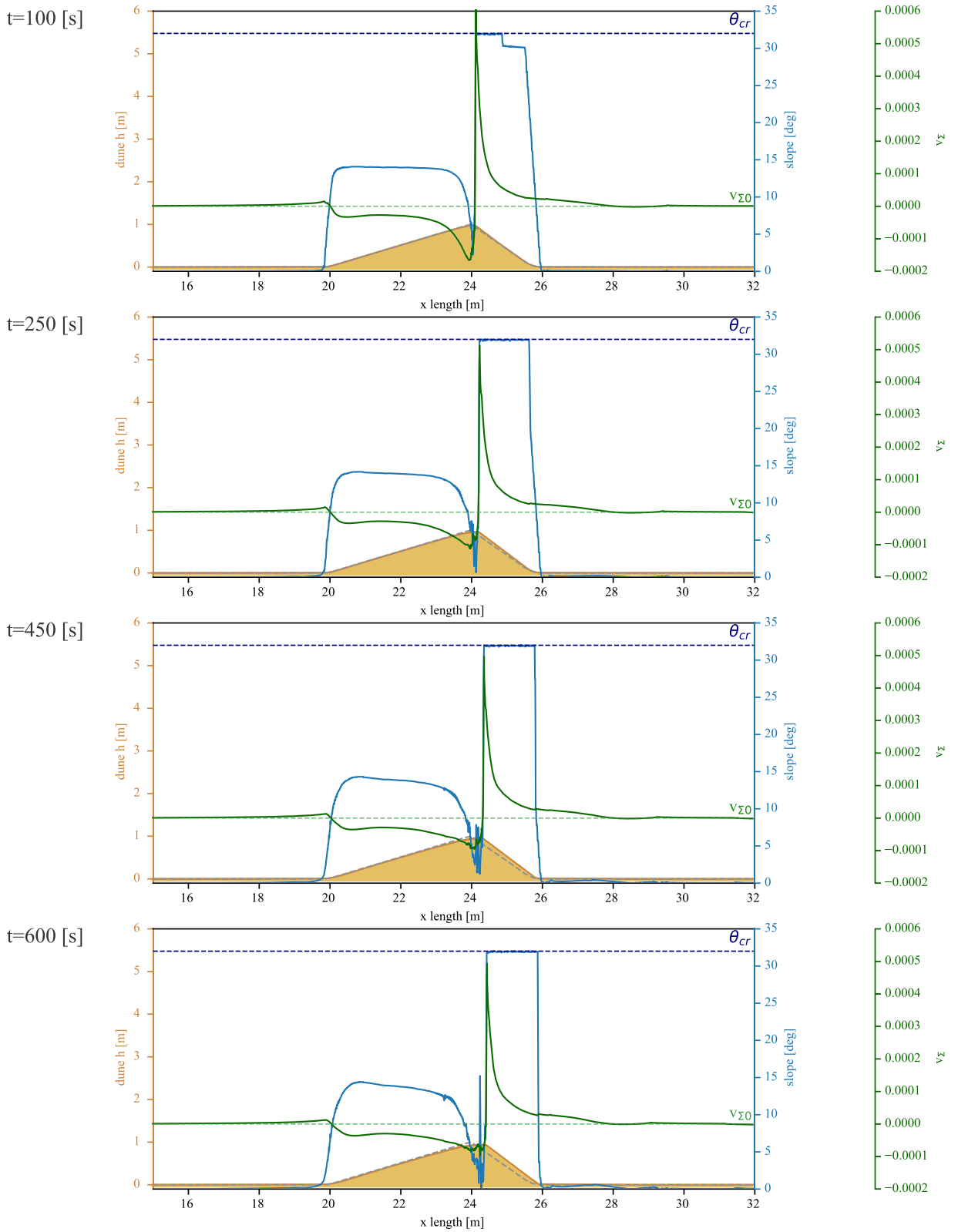


**Fig. 7.** Dune profile (yellow), slope (blue), and $v_\Sigma^{ED}$ (green) at different time steps. Dashed lines represent reference levels: initial dune profile (gray), repose angle (blue), erosion-deposition equilibrium (green). (For interpretation of the references to color in this figure legend, the reader is referred to the web version of this article.)

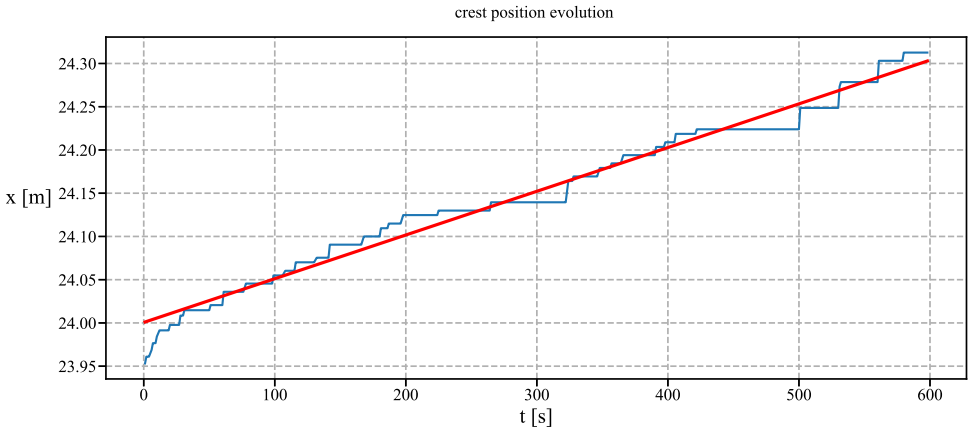


**Fig. 8.** Mean crest position highlighting a nearly constant migration speed after an initial transient of about 20 s.

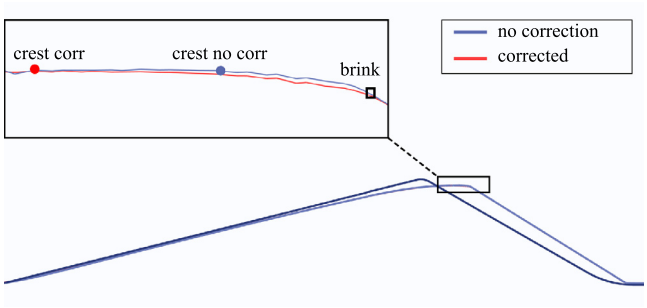


**Fig. 9.** Comparison of the dune configuration at $t = 600$ s with and without the slope-sensitive $u_t^*$ model correction; that is, Eq. (4). The zoomed panel highlights the crest-brink separation obtained with the modified model.

Finally, to look at the phenomena from a global point of view, in Fig. 8 the dune crest advancing velocity is plotted. After an initial transient, it looks uniform as predicted from experimental data and simplified models. However, the model parameters have to be tuned to match the experimental data for real dunes. Only data for much higher dunes are available; therefore, for rigorous matching based on migration speed, a simulation with a much larger domain is required.

To analyze the influence of the slopes on the friction velocity, that is, of Eq. (4), we compare in Fig. 9 the results of the simulations of the two-dimensional dune with the corrected model and with the slope-independent model. From a global point of view, the behavior is the same. However, some differences can be noted close to the crest of the dune: the zone is subject to a fast evolution and to several inclination changes. Looking in detail at the differences, we see the slope-sensitive modification promotes the crest-brink separation. This effect is typical of real dunes (see [8,75]), but it is almost always ignored in dune aerodynamic studies, which assume idealized triangular shapes. The effect will be bigger in a three-dimensional simulation, because the effective angle $\vartheta$ does not vanish in general.

### 3.2. Three-dimensional dune simulation: from a symmetric Gaussian pile to a barchan

As a second numerical test we selected a three-dimensional case, using Eq. (5), to correct the evaluation of $u_t^*$. As mentioned in Section 1, this kind of case has been the subject of dedicated models (e.g., [33–35,49]). The initial sand pile surface is a symmetric Gaussian as represented in Fig. 10, with maximum height $h_M = 0.5$ m, a setup similar to that used in [49]. However, as mentioned in Section 1, that model avoids the explicit computation of sand saltation and suspension, using a simple model to describe the motion of the dune.

Dunes of this kind are also known as *downsized crescent-shaped dunes* because the sizes considered are typical of wind-tunnel-scale crescent-shaped bedforms (see, e.g., [70,76–79]). The dune size used herein is too large to be reproduced in most existing wind tunnels, and is closer to the real dune size (the minimum size of an observed barchan is 1 m [76,78,80]) observed in desert areas subjected to an almost persistent wind direction.

The same boundary conditions as for the two-dimensional simulation were used, while for lateral boundary surfaces, symmetry conditions were imposed.

The transport mechanism and translation are the same as reported in Fig. 3 for the two-dimensional case, even though three-dimensional wind effects play a crucial role in the particular shape assumed by the sand pile. Under the action of the

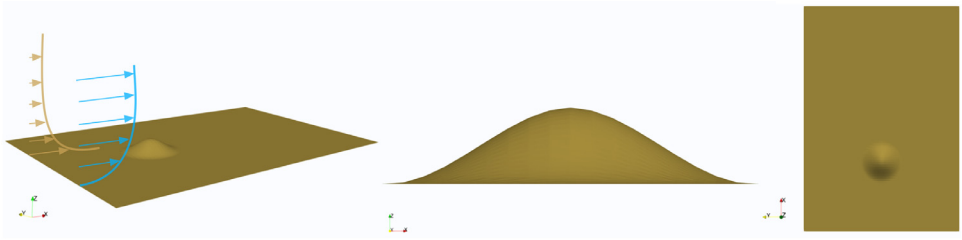


**Fig. 10.** Initial sand-bed configuration for the three-dimensional simulation of a dune: (a) global view with inlet profiles; (b) horizontal section; (c) top view.

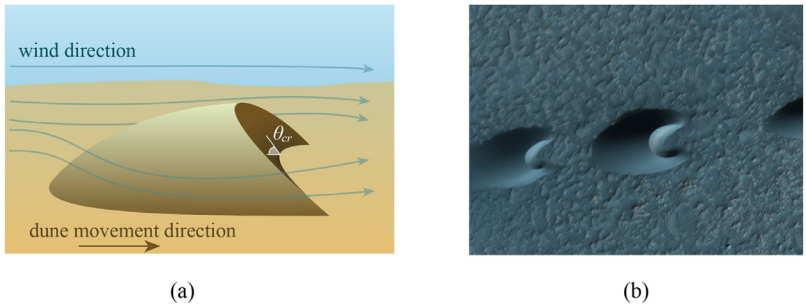


**Fig. 11.** (a) Barchan sketch. (b) Barchans on Mars (from Wikipedia).

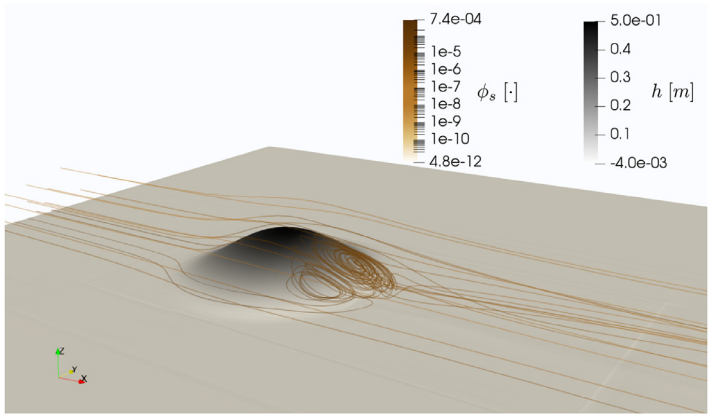


**Fig. 12.** Streamlines around the dune at $t = 80$ s, colored on the basis of the sand volume fraction $\phi_s$. In the wake and on the lateral sides, the wind is not directed along the local steepest-slope direction of the surface; therefore, it feels an effective angle that is different form the local slope of the surface. The sand surface is colored according to the height (gray scale). (For interpretation of the references to color in this figure legend, the reader is referred to the web version of this article.)

wind, the shape is modified, tending to a barchan crescent-shaped dune presenting a steep downwind face, with two *horns* pointing downwind as sketched in Fig. 11(a).

Zhou et al. [49] used the modification for $u_t^*$ reported in Eq. (4) proposed by Iversen and Rasmussen [25], which does not take into account the effective angle between the wind direction and the sand surface as done in Eq. (5). Of course, as shown in Fig. 12, which shows the streamlines around the dune at $t = 80$ s, in this case the streamlines close to the pile surface are not parallel to the steepest-slope direction, so the correction (5) should be used to get more accurate results.

Fig. 13 compares the initial sand pile shape with the state reached after 145 s. The evolution of the shape is a slow process, and the larger the dune, the slower the evolution velocity. With this in mind, Fig. 13(b) should be compared with Fig. 7(b) in [78], which shows the experimental top view of a 20-cm height sand pile evolution.

The surface velocity $\mathbf{v}_\Sigma^{ED}$ contours reported in Fig. 14 well explain how this process leads to this particular shape. The sand is eroded from all over the upwind face, and the deposition is maximum rigth after the crest, with a C-shaped profile, which forms two symmetric preferential directions for avalanche flux, leading to the typical horns of barchans. Moreover, the lateral parts of the initial hill are smaller than the center of the Gaussian, and the migration velocity of an along-wind

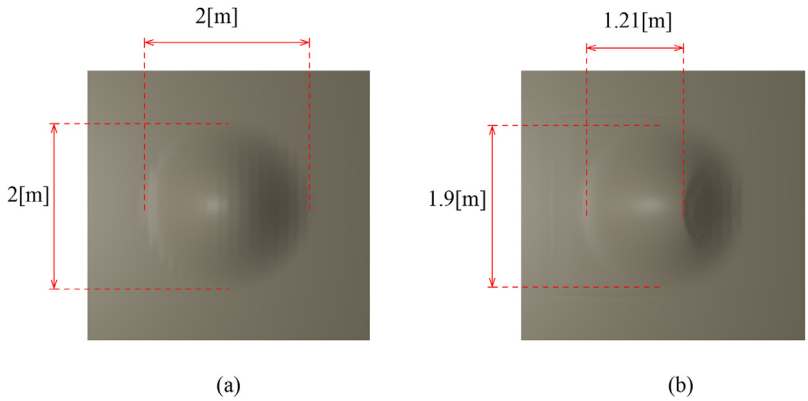


**Fig. 13.** Top view of the initial sand pile (a) and shape after 145 s (b).

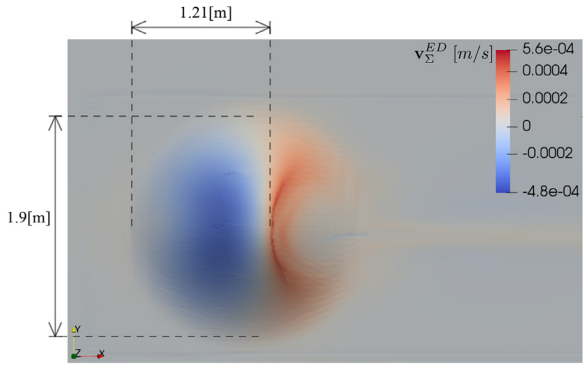


**Fig. 14.** $\mathbf{v}_\Sigma^{ED}$ on the sand surface at $t = 80$ s. Erosion-deposition fluxes modify the surface, which starts to appear similar to a barchan shape. In particular, the deposition peak immediately after the crest and the linked avalanche surface flux cause the formation of lateral horns.

longitudinal slice of the hill scales with the inverse of the slice's size. Therefore, the lateral parts move faster than the crest. Even though the main features of the evolution are well reproduced, the shape assumed at the end of the simulation (145 s) is not a stable-equilibrium configuration. The dune height is slightly decreased. A longer simulation time is required to investigate the long-term behavior, and this will be addressed in future work.

### *3.3. Windblown sand transport hindered by a vertical wall*

The last numerical simulation deals with a straight vertical wall that might be used for windblown sand mitigation. Although for the previously presented cases other models have been developed (even though they use approximations on the wind flow treatment, especially in the wake of the dunes), in this last part we present situations in which the effective sand transport in air has to be explicitly simulated by means of a multiphase approach. Such an example is suggested by civil engineering interests in testing such kinds of devices (e.g., [45–48,81]). In the same context, at the end of the section we show that the model can be used to simulate other nonstandard sandy flows interacting with different obstacles, such as a porous barrier and a ditch.

The vertical wall presents two main features that can be handled by the proposed model:

1. The bluff body induces recirculation bubbles both upwind and downwind (see [47]). Such generated flow structures require the flow to be solved accurately and cannot be predicted by perturbation theory. Moreover, the air-flow modeling approach and the turbulence model should be selected accurately. As stated earlier, the $k - \omega$ SST turbulence model has been used by different authors for the same class of problem (e.g., [29,47]) and has been fully validated [31].
2. The presence of the obstacle makes the already developed models for dune evolution not directly applicable to this case. The complex suspension transport mode is crucial to evaluate the amount of sand trapped by the mitigation measure, the amount of sand overcoming it, and where it deposits upwind.

Such a case is analogous to one of the configurations studied in a wind tunnel for a particular barrier's shape in [46].

The configuration studied is shown in Fig. 15. The barrier is 1 m high. At the beginning of the simulation, an initial amount of sand is placed in front of the barrier, with a straight profile inclined at an angle of about 11°. Two recirculation

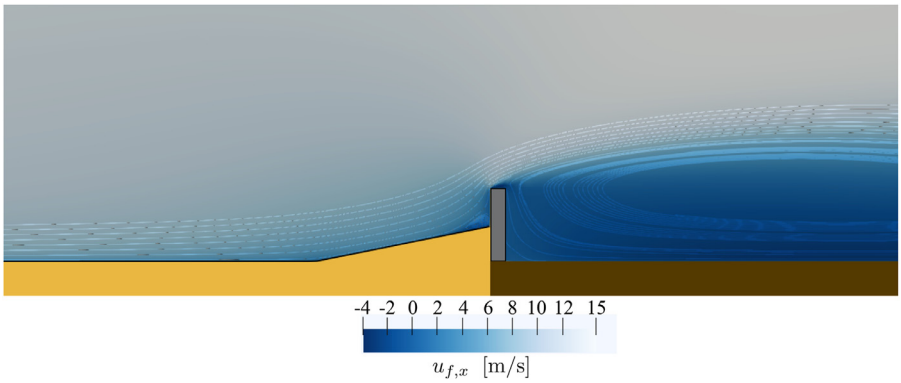


**Fig. 15.** Vertical wall with initial pile of accumulated sand. The sandy terrain is colored yellow. Brown indicates the ground sand-free. The horizontal wind velocity field is reported with the streamlines around the barrier. (For interpretation of the references to color in this figure legend, the reader is referred to the web version of this article.)

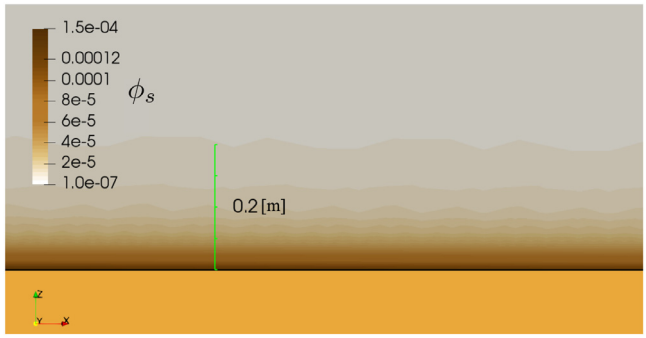


**Fig. 16.** Saltation layer upwind of the barrier. Its height evaluated with the criterion (9) is about 20 cm as commonly observed in reality.

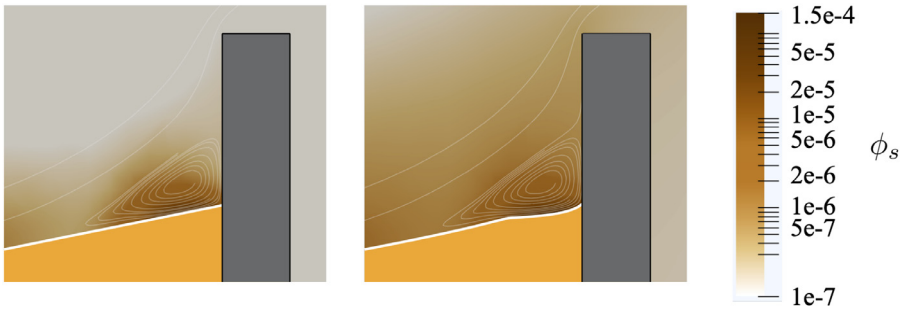


**Fig. 17.** Initial and final sand profile and sand volume ratio around the barrier. The upwind vortex generated by the barrier is altered by the ground evolution.

bubbles are generated: a bigger one in the wake of the barrier, and a small eddy upwind. The saltation layer is accurately reproduced and is reported in Fig. 16. As for the barrier studied in [46], the wind flow digs the sand, altering the initial straight profile, as shown in Fig. 17, which compares initial and final shapes of the sand pile upwind of the barrier. It is interesting to note the mutual effect of wind and sand: the shear stress generated by the upwind vortex is capable of eroding a certain amount of sand; this process alters the shape of the sand profile, which consequently affects the shape of the bubble. The profile after 145 s shows an analogous modification induced by the upwind vortex observed in a wind tunnel for a different barrier [46].

Looking at the final state, we clearly see that a certain amount of sand entrained in the air is capable of overcoming the wall. From a quantitative point of view, this amount of mass can be obtained by integrating along a vertical line the normal sand flux $q_{s,x} = u_{tr,x}\phi_s\hat{\rho}_s$, obtaining the integral sand drift, which can be used to evaluate the efficiency of the barrier as a sand mitigation measure.

In the same spirit, other mitigation measures can be studied, such as the ones reported in Fig. 18: a 40% porosity barrier and a ditch. Fig. 18 shows the wind velocity magnitude, the turbulent kinetic energy, and the sand volume ratio in the air.

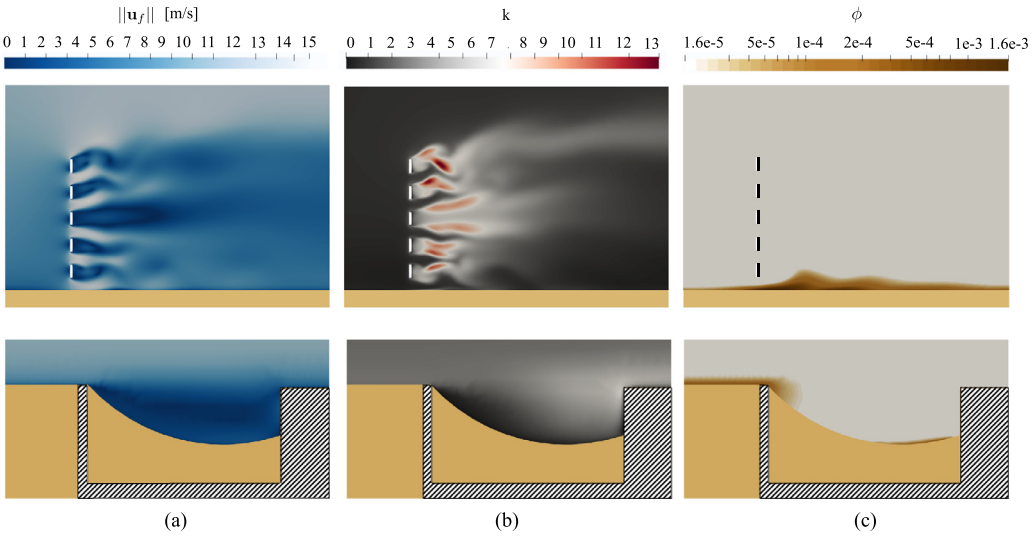


**Fig. 18.** (a) Wind velocity magnitude, (b) turbulent kinetic energy, and (c) sand volume fraction for a porous barrier with horizontal slats (first row) and a ditch (second row).

The porous fence generates complicated flow patterns in the wake that are hard to approximate and are strongly affected by the porosity [56].

Concerning the ditch shown in Fig. 18 (bottom row), from a pure aerodynamic point of view, as the sand fills the ditch, the vortex inside changes in shape and size, altering the shear stress at the ground and consequently the erosion. Moreover, the presence of an obstacle makes the suspension transport relevant, especially in light of the application for which this artifact is built.

## 4. Conclusions

The fully Eulerian model proposed in this article is able to describe the motion of windblown sand in the air and the evolution of the sand bed. It takes into account the main physical phenomena contributing to sand transport at medium and large scales: erosion, saltation and suspension transport, sedimentation, and avalanching. In this way it is capable of dealing with the morphological changes present both in complex natural phenomena such as dune migration dynamics and in the interactions with human-built artifacts such as obstacles. This feature is particularly interesting for engineering applications when the interaction between sand and infrastructures needs be studied. An example is the identification of sand mitigation devices, the evaluation of their efficacy, and the evaluation of the regions where sand accumulates.

The proposed model solves for the wind flow fields, allowing one to simulate situations in which complicated flow structures are generated. Moreover, the model explicitly computes the concentration of sand in the air due to the suspension transport mode, the interaction of particles among themselves in the saltation layer, the erosion/deposition fluxes, and the sliding of grains, resulting in the evolution of the ground surface.

At the cost of increased complexity of the model, the accuracy of the interaction between the phases could be increased by considering momentum balance equations for the dispersed phase, both in a monodisperse case and in a polydisperse case. This modification might become particularly relevant very close to the ground, where saltation occurs and sand concentration is the highest. Moreover, creep and reptation bed flux could be included as well. These improvements could be useful for small-scale modeling and simulations.

The same physical laws govern other particulate transport phenomena. With some obvious changes and adaptations, the same modeling approach could be extended to the transport and deposition of other particulate windblown flows, such as snow, rain, and volcanic ashes.

## Acknowledgments

The authors thank L. Bruno, R. Nuca, and N. Coste, members of the Windblown Sand Modeling and Mitigation Joint Research, Development and Consulting Group established between the Politecnico di Torino and Optiflow, and H. Jasak and his research group at the University of Zagreb for helpful discussions of the topics of this article. This research was supported in part by the Istituto Nazionale di Alta Matematica and Regione Piemonte. The research activity was developed within the MSCA-ITN-2016-EID SMaRT research project. This project received funding from the European Union's Horizon 2020 research and innovation program (grant agreement no. 721798).

## References


[1] J. Kok, E. Parteli, T. Michaels, D. Karam, The physics of wind-blown sand and dust, Rep. Prog. Phys. 75 (10) (2012) 106901.
[2] R. Bagnold, The Physics of Blown Sand and Desert Dunes, Methuen & Company, 1941.
[3] R. Anderson, P. Haff, Simulation of eolian saltation, Science 241 (4867) (1988) 820–823.
[4] G. Sauermann, K. Kroy, H. Herrmann, Continuum saltation model for sand dunes, Phys. Rev. E 64 (3) (2001) 031305.
[5] K. Kroy, G. Sauermann, H.J. Herrmann, Minimal model for aeolian sand dunes, Phys. Rev. E 66 (3) (2002) 031302.
[6] G. Sauermann, J. Andrade, L. Maia, U. Costa, A. Araújo, H. Herrmann, Wind velocity and sand transport on a barchan dune, Geomorphology 54 (3–4) (2003) 245–255, doi:10.1016/S0169-555X(02)00359-8.
[7] B. Andreotti, A two-species model of aeolian sand transport, J. Fluid Mech. 510 (2004) 47–70, doi:10.1017/S0022112004009073.
[8] E. Parteli, V. Schwämmle, H. Herrmann, L. Monteiro, L. Maia, Profile measurement and simulation of a transverse dune field in the Lençóis Maranhenses, Geomorphology 81 (1–2) (2006) 29–42.
[9] M. Pischiutta, L. Formaggia, F. Nobile, Mathematical modelling for the evolution of aeolian dunes formed by a mixture of sands: entrainment-deposition formulation, Commun. Appl. Ind. Math. 2 (2) (2011), doi:10.1685/journal.caim.377.
[10] A. Lo Giudice, R. Nuca, L. Preziosi, N. Coste, Wind-blown particulate transport: a review of computational fluid dynamics models, Math. Eng. 1 (3) (2019) 508–547.
[11] L. Kang, Discrete particle model of aeolian sand transport: comparison of 2D and 2.5D simulations, Geomorphology 139 (2012) 536–544, doi:10.1016/j.geomorph.2011.12.005.
[12] L. Kang, L. Guo, Eulerian–Lagrangian simulation of aeolian sand transport, Powder Technol. 162 (2) (2006) 111–120.
[13] L. Kang, D. Liu, Numerical investigation of particle velocity distributions in aeolian sand transport, Geomorphology 115 (1–2) (2010) 156–171.
[14] A. Lopes, L. Oliveira, A.D. Ferreira, J. Pinto, Numerical simulation of sand dune erosion, Environ. Fluid Mech. 13 (2) (2013) 145–168, doi:10.1007/s10652-012-9263-2.
[15] D. Tong, N. Huang, Numerical simulation of saltating particles in atmospheric boundary layer over flat bed and sand ripples, J. Geophys. Res. Atmos. 117 (2012) D16205.
[16] Z. Li, Y. Wang, Y. Zhang, A numerical study of particle motion and two-phase interaction in aeolian sand transport using a coupled large eddy simulation - discrete element method, Sedimentology 61 (2) (2014) 319–332, doi:10.1111/sed.12057.
[17] H. Jiang, H. Dun, D. Tong, N. Huang, Sand transportation and reverse patterns over leeward face of sand dune, Geomorphology 283 (2017) 41–47.
[18] X. Shi, P. Xi, J. Wu, A lattice Boltzmann-saltation model and its simulation of aeolian saltation at porous fences, Theor. Comput. Fluid Dyn. 29 (1–2) (2015) 1–20, doi:10.1007/s00162-014-0338-1.
[19] F. Xiao, L. Guo, D. Li, Y. Wang, Discrete particle simulation of mixed sand transport, Particuology 10 (2) (2012) 221–228, doi:10.1016/j.partic.2011.10.004.
[20] S. Alhajraf, Numerical simulation of drifting sand, Cranfield University, 2000 (Ph.D. thesis).
[21] S. Ji, A. Gerber, A. Sousa, A convection-diffusion CFD model for aeolian particle transport, Int. J. Numer. Methods Fluids 45 (8) (2004) 797–817, doi:10.1002/fld.724.
[22] L. Preziosi, D. Fransos, L. Bruno, A multiphase first order model for non-equilibrium sand erosion, transport and sedimentation, Appl. Math. Lett. 45 (2015) 69–75, doi:10.1016/j.aml.2015.01.011.
[23] A. Lo Giudice, G. Giammanco, D. Fransos, L. Preziosi, Modelling sand slides by a mechanics-based degenerate parabolic equation, Math. Mech. Solids (2018) ., doi:10.1177/1081286518755230.
[24] L. Raffaele, L. Bruno, F. Pellerey, L. Preziosi, Windblown sand saltation: a statistical approach to fluid threshold shear velocity, Aeolian Res. 23 (2016) 79–91.
[25] J. Iversen, K. Rasmussen, The effect of wind speed and bed slope on sand transport, Sedimentology 46 (4) (1999) 723–731, doi:10.1046/j.1365-3091.1999.00245.x.
[26] D. Parsons, I. Walker, G. Wiggs, Numerical modelling of flow structures over idealized transverse aeolian dunes of varying geometry, Geomorphology 59 (1–4) (2004a) 149–164, doi:10.1016/j.geomorph.2003.09.012.
[27] D. Parsons, G. Wiggs, I. Walker, R. Ferguson, B. Garvey, Numerical modelling of airflow over an idealised transverse dune, Environ. Model. Softw. 19 (2) (2004b) 153–162, doi:10.1016/S1364-8152(03)00117-8.
[28] V. Schatz, H. Herrmann, Flow separation in the lee side of transverse dunes: a numerical investigation, Geomorphology 81 (1–2) (2006) 207–216.
[29] B. Liu, J. Qu, W. Zhang, G. Qian, Numerical simulation of wind flow over transverse and pyramid dunes, J. Wind Eng. Ind. Aerodyn. 99 (8) (2011) 879–888.
[30] A. Araújo, E. Parteli, T. Pöschel, J. Andrade, H. Herrmann, Numerical modeling of the wind flow over a transverse dune, Sci. Rep. 3 (2858) (2013) 1–9, doi:10.1038/srep02858.
[31] L. Bruno, D. Fransos, Sand transverse dune aerodynamics: 3D coherent flow structures from a computational study, J. Wind Eng. Ind. Aerodyn. 147 (2015) 291–301.
[32] O. Durán, E.J. Parteli, H.J. Herrmann, A continuous model for sand dunes: review, new developments and application to barchan dunes and barchan dune fields, Earth Surf. Process. Landf. 35 (13) (2010) 1591–1600.
[33] V. Schwämmle, H.J. Herrmann, Geomorphology: solitary wave behaviour of sand dunes, Nature 426 (6967) (2003) 619.
[34] V. Schwämmle, H. Herrmann, A model of barchan dunes including lateral shear stress, Eur. Phys. J. E 16 (1) (2005) 57–65.
[35] O. Durán, V. Schwämmle, H. Herrmann, Breeding and solitary wave behavior of dunes, Phys. Rev. E 72 (2) (2005) 021308.
[36] O. Durán, H.J. Herrmann, Vegetation against dune mobility, Phys. Rev. Lett. 97 (2006) 188001, doi:10.1103/PhysRevLett.97.188001.
[37] O. Durán, L.J. Moore, Vegetation controls on the maximum size of coastal dunes, Proc. Natl. Acad. Sci. USA 110 (43) (2013) 17217–17222, doi:10.1073/pnas.1307580110.
[38] E.J.R. Parteli, H.J. Herrmann, Saltation transport on Mars, Phys. Rev. Lett. 98 (2007) 198001, doi:10.1103/PhysRevLett.98.198001.
[39] E.J.R. Parteli, O. Durán, H. Tsoar, V. Schwämmle, H.J. Herrmann, Dune formation under bimodal winds, Proc. Natl. Acad. Sci. USA 106 (52) (2009) 22085–22089, doi:10.1073/pnas.0808646106.
[40] E.J.R. Parteli, J.S. Andrade, H.J. Herrmann, Transverse instability of dunes, Phys. Rev. Lett. 107 (2011) 188001, doi:10.1103/PhysRevLett.107.188001.
[41] D. Zhang, C. Narteau, O. Rozier, S. Courrech du Pont, Morphology and dynamics of star dunes from numerical modelling, Nat. Geosci. 5 (7) (2012) 463, doi:10.1038/ngeo1503.
[42] X. Gao, C. Narteau, O. Rozier, S.C. Du Pont, Phase diagrams of dune shape and orientation depending on sand availability, Sci. Rep. 5 (2015) 14677, doi:10.1038/srep14677.
[43] A. Farimani, A. Ferreira, A. Sousa, Computational modeling of the wind erosion on a sinusoidal pile using a moving boundary method, Geomorphology 130 (3–4) (2011) 299–311.
[44] E.J.R. Parteli, K. Kroy, H. Tsoar, J.S. Andrade, T. Pöschel, Morphodynamic modeling of aeolian dunes: review and future plans, Eur. Phys. J. Spec. Top. 223 (11) (2014) 2269–2283.
[45] S. Hotta, K. Horikawa, Function of sand fence placed in front of embankment, in: Coastal Engineering 1990, American Society of Civil Engineers, New York, NY, 1991, pp. 2754–2767.
[46] L. Bruno, N. Coste, D. Fransos, A. Lo Giudice, L. Preziosi, L. Raffaele, Shield for sand: an innovative barrier for windblown sand mitigation, Recent Pat. Eng. 12 (3) (2018a) 237–246.
[47] L. Bruno, D. Fransos, A. Lo Giudice, Solid barriers for windblown sand mitigation: aerodynamic behavior and conceptual design guidelines, J. Wind Eng. Ind. Aerodyn. 173 (2018b) 79–90.

[48] L. Bruno, M. Horvat, L. Raffaele, Windblown sand along railway infrastructures: a review of challenges and mitigation measures, J. Wind Eng. Ind. Aerodyn. 177 (2018c) 340–365.
[49] X. Zhou, Y. Zhang, Y. Wang, M. Li, 3D numerical simulation of the evolutionary process of aeolian downsized crescent-shaped dunes, Aeolian Res. 21 (2016) 45–52.
[50] B. Werner, Eolian dunes: computer simulations and attractor interpretation, Geology 23 (12) (1995) 1107–1110, doi:10.1130/0091-7613(1995)023<1107:EDCSAA>2.3.CO;2.
[51] H. Nishimori, M. Yamasaki, A simple model for the various pattern dynamics of dunes, Int. J. Mod. Phys. B 12 (03) (1998) 257–272, doi:10.1142/S021797929800020X.
[52] A. Katsuki, H. Nishimori, N. Endo, K. Taniguchi, Collision dynamics of two barchan dunes simulated using a simple model, J. Phys. Soc. Jpn. 74 (2) (2005) 538–541.
[53] C. Narteau, D. Zhang, O. Rozier, P. Claudin, Setting the length and time scales of a cellular automaton dune model from the analysis of superimposed bed forms, J. Geophys. Res. Earth Surf. 114 (F3) (2009) F03006, doi:10.1029/2008JF001127.
[54] N. Zhang, J.H. Kang, S.J. Lee, Wind tunnel observation on the effect of a porous wind fence on shelter of saltating sand particles, Geomorphology 120 (3–4) (2010) 224–232.
[55] N. Zhang, S.J. Lee, T.G. Chen, Trajectories of saltating sand particles behind a porous fence, Geomorphology 228 (2015) 608–616.
[56] B. Li, D.J. Sherman, Aerodynamics and morphodynamics of sand fences: a review, Aeolian Res. 17 (2015) 33–48.
[57] J.J. Cheng, J.Q. Lei, S.Y. Li, H.F. Wang, Disturbance of the inclined inserting-type sand fence to wind–sand flow fields and its sand control characteristics, Aeolian Res. 21 (2016) 139–150.
[58] F. Menter, Two-equation eddy-viscosity turbulence models for engineering applications, AIAA J. 32 (8) (1994) 1598–1605.
[59] F. Menter, M. Kuntz, R. Langtry, Ten years of industrial experience with the SST turbulence model, Turbul. Heat Mass Transf. 4 (1) (2003) 625–632.
[60] F. Menter, Zonal two equation kw turbulence models for aerodynamic flows, in: Proceedings of the Twenty-third Fluid Dynamics, Plasmadynamics, and Lasers Conference, 1993, p. 2906.
[61] S. Balachandar, J. Eaton, Turbulent dispersed multiphase flow, Annu. Rev. Fluid Mech. 42 (2010) 111–133.
[62] E. Barnea, J. Mizrahi, A generalized approach to the fluid dynamics of particulate systems: part 1. General correlation for fluidization and sedimentation in solid multiparticle systems, Chem. Eng. J. 5 (2) (1973) 171–189, doi:10.1016/0300-9467(73)80008-5.
[63] P. Brown, D. Lawler, Sphere drag and settling velocity revisited, J. Environ. Eng. 129 (3) (2003) 222–231.
[64] E. Farrell, D. Sherman, A new relationship between grain size and fall (settling) velocity in air, Prog. Phys. Geogr. 39 (3) (2015) 361–387.
[65] G. Bagheri, C. Bonadonna, On the drag of freely falling non-spherical particles, Powder Technol. 301 (2016) 526–544.
[66] Y. Shao, H. Lu, A simple expression for wind erosion threshold friction velocity, J. Geophys. Res. Atmos. 105 (D17) (2000) 22437–22443, doi:10.1029/2000JD900304.
[67] T. Ho, P. Dupont, A. El Moctar, A. Valance, Particle velocity distribution in saltation transport, Phys. Rev. E 85 (5) (2012) 052301, doi:10.1103/PhysRevE.85.052301.
[68] T. Ho, A. El Moctar, P. Dupont, Scaling laws in aeolian sand transport, Phys. Rev. Lett. 106 (9) (2013) 094501.
[69] T.D. Ho, A. Valance, P. Dupont, A. El Moctar, Aeolian sand transport: Length and height distributions of saltation trajectories, Aeolian Res. 12 (2014) 65–74.
[70] R. Faria, A. Ferreira, J. Sismeiro, J. Mendes, A. Sousa, Wind tunnel and computational study of the stoss slope effect on the aeolian erosion of transverse sand dunes, Aeolian Res. 3 (3) (2011) 303–314, doi:10.1016/j.aeolia.2011.07.004.
[71] F.M. Exner, Über die Wechselwirkung zwischen Wasser und Geschiebe in Flüssen, Akad. Wiss Wien Mat.h Nat. 134 (2a) (1925) 165–204.
[72] C. Canuto, A. Lo Giudice, A multi-timestep Robin–Robin domain decomposition method for time dependent advection-diffusion problems, Appl. Math. Comput. 363 (2018) 124596.
[73] P. Richards, S. Norris, Appropriate boundary conditions for computational wind engineering models revisited, J. Wind Eng. Ind. Aerodyn. 99 (4) (2011) 257–266.
[74] B. Blocken, T. Stathopoulos, J. Carmeliet, CFD simulation of the atmospheric boundary layer: wall function problems, Atmos. Environ. 41 (2) (2007) 238–252.
[75] G. Sauermann, P. Rognon, A. Poliakov, H. Herrmann, The shape of the barchan dunes of southern Morocco, Geomorphology 36 (1–2) (2000) 47–62.
[76] P. Hersen, S. Douady, B. Andreotti, Relevant length scale of barchan dunes, Phys. Rev. Lett. 89 (26) (2002) 264301.
[77] O. Dauchot, F. Lechénault, C. Gasquet, F. Daviaud, “Barchan” dunes in the lab, Compt. Rend. Mech. 330 (3) (2002) 185–191.
[78] B. Andreotti, P. Claudin, S. Douady, Selection of dune shapes and velocities part 1: dynamics of sand, wind and barchans, Eur. Phys. J. B 28 (3) (2002) 321–339.
[79] Y. Zhang, Y. Wang, P. Jia, Evolution of downsized crescent-shaped dune in wind tunnel experiment, Sci. China Phys. Mech. 57 (1) (2014) 143–151.
[80] S. Hastenrath, The barchan dunes of southern Peru revisited, Z. Geomorphol. 31 (1987) 167–178.
[81] S. Zhang, G.D. Ding, M.H. Yu, G.L. Gao, Y.Y. Zhao, L. Wang, Y.Z. Wang, Application of boundary layer displacement thickness in wind erosion protection evaluation: case study of a Salix psammophila sand barrier, Int. J. Environ. Res. Public Health 16 (2019) 592, doi:10.3390/ijerph16040592.